

Microstructure evolution of the laser surface melted WC-Ni coatings exposed to cavitation erosion

Ziqi Xu^{a,b,c,1}, Ye Tian^{b,c,1}, Xiaomei Liu^{b,c,1}, Rui Yang^{b,c}, Hua Li^{b,c}, Xiuyong Chen^{b,c,*}

^a Faculty of Materials Metallurgy and Chemistry, Jiangxi University of Science and Technology, Ganzhou 341000, China

^b Key Laboratory of Marine Materials and Related Technologies, Zhejiang Key Laboratory of Marine Materials and Protective Technologies, Ningbo Institute of Materials Technology and Engineering, Chinese Academy of Sciences, Ningbo 315201, China

^c Zhejiang Engineering Research Center for Biomedical Materials, Cixi Institute of Biomedical Engineering, Ningbo Institute of Materials Technology and Engineering, Chinese Academy of Sciences, Ningbo 315201, China

ARTICLE INFO

Keywords:

Cermet
Coating
Cavitation
Scanning electron microscopy

ABSTRACT

In this study, WC-Ni coatings were deposited using cold spraying followed by laser surface melting to improve the cavitation erosion resistance. The remelted coating presented a three-dimensional WC skeleton structure which could be regulated. The remelted coatings with uniformly distributed WC skeleton exhibited remarkable cavitation erosion resistance. The observed microstructure evolution in the remelted coatings during cavitation erosion suggested that the WC skeleton prevented crack propagation and therefore enhanced the cavitation erosion resistance. Results also indicated that the enhanced cavitation erosion resistance of the remelted coatings was attributed to the synergistic effect of the Ni binder phase and the hard WC phase. Adjusting and controlling the structure of the coatings allowed the WC-based coatings to exhibit excellent cavitation erosion resistance.

1. Introduction

In the last several decades, global warming caused by carbon emissions has become a serious threat to the survival of human beings and animals [1–3]. Due to the considerable proportion of the global CO₂ emissions from fossil-fuel power generation [4,5], a low-carbon alternative to fossil fuels was essential. Hydropower is one of the most popular renewable energy resources to produce electricity [6,7]. However, various failures in hydraulic turbines restricted the development of hydropower, among which cavitation erosion is the major failure mode [8]. To extend the service life of the blades of hydraulic turbines, the methods of improving cavitation erosion resistance of materials have been studied widely [9,10].

WC-based coatings are considered to provide effective cavitation erosion resistance to hydraulic turbine blades due to their high hardness and toughness [11,12]. The high hardness is mainly attributed to the hard WC phase, while the toughness is dependent on the metallic binder phase, and the cavitation erosion resistance is relative to both phases. It is proposed that the cavitation erosion resistance of the WC-based coatings can be enhanced by the increase of toughness via increasing

the binder phase content [13,14]. However, the damage by cavitation erosion is more common at the interface between the unmelted WC particles and the metal matrix [15]. It is also reported that the crack propagation in the binder phase is much easier than that in the hard phase. These cracks would cause the removal of the WC particles, leading to severe cavitation erosion damage [16,17]. For better performance of WC-based coatings in cavitation erosion resistance, an appropriate microstructure that overcomes the drawbacks of the metallic binder phase and hard WC phase in cavitation erosion is strongly needed.

Laser surface remelting is one of the feasible methods to improve the surface quality of the coatings [18,19]. The coatings with a homogeneous microstructure, which can have a positive effect on cavitation erosion resistance, can be fabricated by laser surface remelting [20–22]. In addition, the cooling rate of the remelted layer during the laser surface remelting is much higher than that obtained during the casting process [23]. Such a high cooling rate in the remelting layer could produce microstructures different from casting. For example, thermal-sprayed WC-Co coatings processed by surface melting exhibited unique microstructures, which provided improved hardness and wear

* Corresponding author at: Key Laboratory of Marine Materials and Related Technologies, Zhejiang Key Laboratory of Marine Materials and Protective Technologies, Ningbo Institute of Materials Technology and Engineering, Chinese Academy of Sciences, Ningbo 315201, China.

E-mail address: chenxiuyong@nimte.ac.cn (X. Chen).

¹ These authors contributed equally: Ziqi Xu, Ye Tian, Xiaomei Liu.

<https://doi.org/10.1016/j.triboint.2022.107615>

Received 5 March 2022; Received in revised form 21 April 2022; Accepted 30 April 2022

Available online 4 May 2022

0301-679X/© 2022 Elsevier Ltd. All rights reserved.

resistance [24,25]. Based on the above studies, it was expected that the laser surface remelting technique could improve the microstructure of the WC-Ni coating to combine the advantages of the hard phase and binder phase, enhancing cavitation erosion resistance. Our previous study found that the WC skeleton structure formed in WC-Ni coating after laser surface remelting, and this structure improved the cavitation erosion resistance [26]. However, the mechanism of the cavitation erosion resistance for the WC-Ni coating with the WC skeleton is not entirely understood yet.

In this study, the cold-sprayed WC-Ni coatings were remelted by laser surface melting at different laser powers. The morphology, microhardness, and phase composition of the as-sprayed coatings and the remelted coatings were investigated. The cavitation erosion resistance of the coatings was measured in deionized water. The surface profile of the specimens after the cavitation erosion test was characterized in terms of arithmetical mean height (S_a) and maximum pit height (S_v). The influence of the microstructure on the cavitation erosion resistance of the coatings was discussed. Furthermore, the microstructure evolution of the remelted layer was investigated to understand the cavitation erosion mechanism better.

2. Experimental procedures

2.1. Material

The cold sprayed WC-Ni coatings were deposited by a low-pressure cold spray system (SST Series P, Centerline, Ltd., Windsor, ON, Canada) onto 316 L stainless steel substrates with a size of Φ 20 mm \times 10 mm. The parameters for cold spraying are listed in Table 1.

Before laser surface remelting, the surface of WC-Ni coatings was ground by abrasive paper and then polished by 0.25 μ m diamond suspension. Specimens were cleaned using alcohol and deionized water then dried in vacuum. The WC-Ni coatings were treated using the Ytterbium laser system (YLS-2000, Han's Laser Technology Co., Ltd., Shenzhen, China) with different laser powers (300, 400, and 500 W), and the specimens were named as 300 W, 400 W, and 500 W coatings, respectively.

2.2. Cavitation erosion test

The cavitation erosion test was conducted by utilizing an ultrasonic fatigue device (GBS-SCT 20 A, Guobiao Ultrasonic Equipment Co., Ltd., Hangzhou, China) in accordance with ASTM G32-16. The schematic diagram of the cavitation erosion test system was shown in our previous work [27]. The rated power of this system was 1500 W, the vibration frequency was 20 ± 0.2 kHz, and the peak-to-peak amplitude was 50 μ m. The test medium was deionized water, and the vibratory horn was immersed in the medium at a depth of 23 ± 2 mm. The specimen was placed under the vibratory horn, and the distance from the vibratory horn to the specimen surface was 1 mm. The temperature of the medium was maintained at $25 \pm 2^\circ\text{C}$ by circulating cooling water. Each specimen was subjected to cavitation erosion for 15 h. The mass of the specimen was weighed by an electronic analytical balance (METTLER 220, TOLEDO Instruments Co., Ltd., Shanghai, China) at each testing cycle of 1 h. Each group of the specimens was tested three times. Here, the

cavitation erosion resistance of the as-sprayed WC-Ni coatings (as the control specimen) and the remelted WC-Ni coating was evaluated.

2.3. Sample characterization

The surface and cross-sectional morphologies of the specimens were observed by scanning electron microscope (SEM, Regulus 8230, Hitachi, Japan). The volume ratio of the WC in the as-sprayed WC-Ni coatings was calculated by processing the SEM images with Image J. Laser surface melted WC-Ni coatings were etched to expose their microstructure before SEM observation. The phase composition of the WC coatings before and after surface remelting was studied by X-ray diffraction (XRD, D8 Advance, Bruker, Germany) using Cu K_α source generated at 40 kV and 40 mA at a scanning speed of 0.02 $^\circ/\text{s}$. The microhardness of the specimens was measured via the Vickers hardness test (Wilson VH3300, Buehler, Germany) with a load of 0.2 kgf, and 15 measurements were taken at random sites for each specimen. The surface profile of the specimens after the cavitation erosion test was observed by a 3D optical profilometer (UP-Lambda, Rtec-Instruments Ltd., USA). Arithmetical mean height (S_a) was calculated from the scanning region (1.9 mm \times 1.2 mm), while maximum pit height (S_v) was calculated from the corresponding Abbott Firestone curve. To record the microstructure evolution during cavitation erosion, a series of SEM images were captured at the same region on the cross-section of the coatings subjected to cavitation erosion for different times.

3. Results and discussion

3.1. Coating microstructure

The cross-sectional morphology of the coatings is presented in Fig. 1. The thickness of the as-sprayed WC-Ni coating was about 760 μ m. Ni was the main phase of the Ni-WC coating, and the WC particles were evenly dispersed in the coating. The volume ratio of WC powder was about $25 \pm 2\%$ (Fig. 1a-1). Meanwhile, a few pores were observed from the magnified image (Fig. 1a-2). The microstructure of the coatings changed after laser surface remelting (Fig. 1a-b). The WC particles transformed into lamellae structure, which built a three-dimensional skeleton structure. The remelted WC-Ni coatings were composed of Ni grains and WC lamellae. The remelted depth of the 300 W, 400 W and 500 W coatings was ~ 80 μ m, ~ 170 μ m, and ~ 260 μ m, respectively (Fig. 1b-1, c-1 and d-1). At a high laser power, the energy input was high and the thermal penetration depth to reach the coating was deep. Therefore, the remelted depth of the 500 W coating was higher than that of the 300 W and 400 W coatings.

The morphology of some WC particles in the remelted layer of the 300 W coating was very similar to that of the WC particles in the as-sprayed coating (Fig. 1a-b), suggesting that the transformation of the WC particles to the WC lamellae under a low laser power of 300 W was incomplete. The incomplete transformation could be attributed to the low laser power, which was insufficient to melt all WC particles. For the 300 W coating, it was also noted that the pores tend to distribute at the WC skeleton area (Fig. 1b-2). By contrast, fewer pores in the WC skeleton area were observed from the 400 W coating (Fig. 1c-2). For the 500 W coating, however, pores were observed at the WC skeleton area and the junction of the WC skeleton and the Ni (Fig. 1d-2). Meanwhile, the size of the pores in the 500 W coating was larger than that in 300 W and 400 W coatings. The existence of the pores could be associated with the air entrapment of the liquid flow during the laser surface remelting. Meanwhile, the reaction of the WC particles with air can lead to decarbonization and the formation of pores [28]. With the insufficient energy input of 300 W, the formation of pores at the WC skeleton area could be associated with the inadequate bonding at the WC/Ni interface and the decarbonization. With the increase of the laser power, the bonding of the WC/Ni interface was improved under high energy input. Therefore, the number of the pores in the remelted layer of 400 W

Table 1
Cold spraying parameters.

Carrier gas	Argon
Carrier gas pressure	483 kPa
Volumetric flow rate of carrier gas	7 NLPm
Compressed gas pressure	634 kPa
Compressed gas temperature	550 $^\circ\text{C}$
Gun velocity	5 mm/s
FMR (flow meter reading)	60
Stand-off distance	5 mm

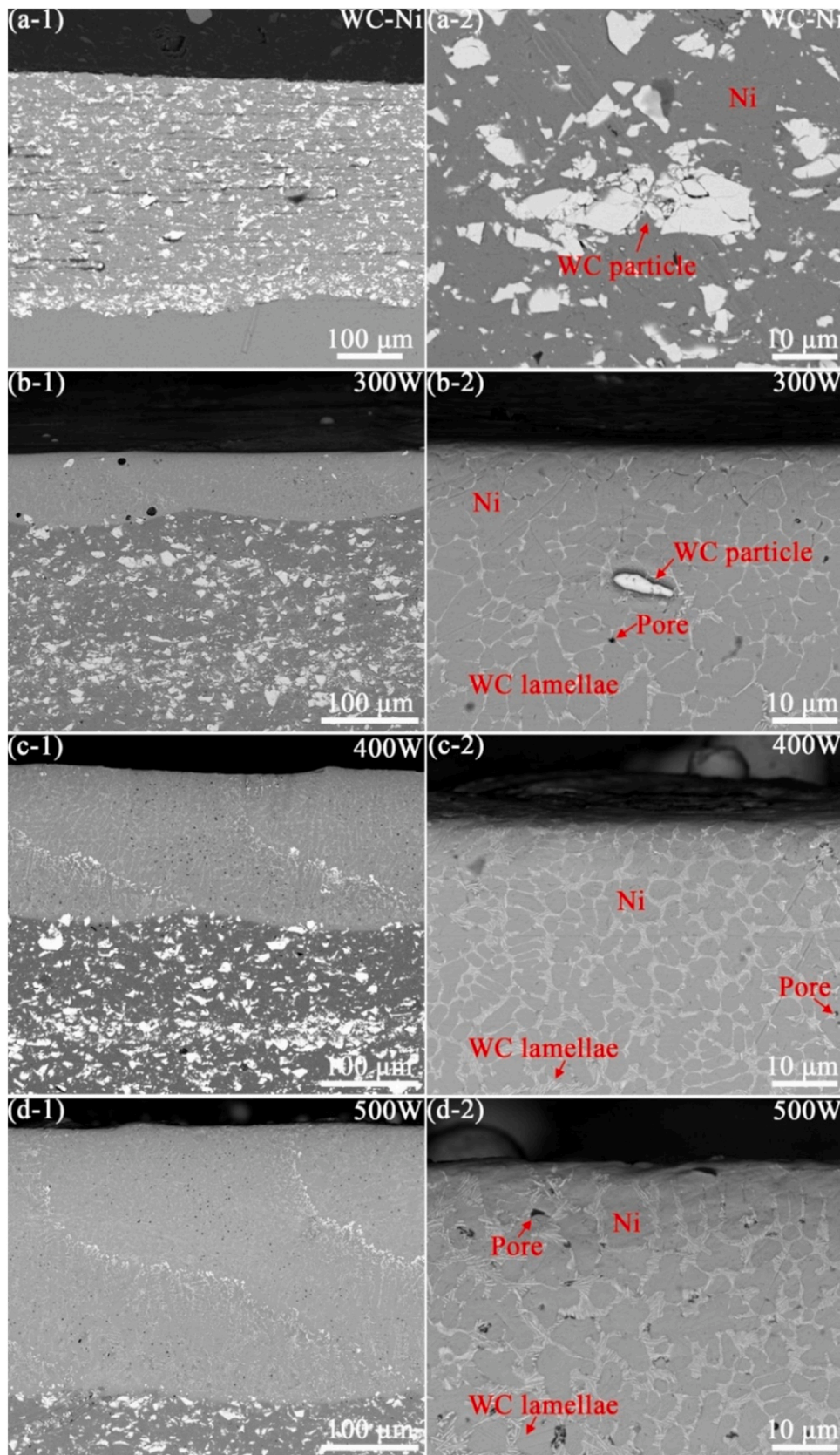


Fig. 1. The cross-sectional morphology of (a) as-sprayed WC-Ni coating and WC-Ni coating after laser surface remelting with (b) 300 W, (c) 400 W, and (d) 500 W laser powers. (-2: enlarged views of the selected area of -1).

coatings decreased. However, the local input energy density was high under 500 W laser power, leading to more unstable melt flow and more pores developed on the remelted layer [29].

Polished surfaces were etched before SEM observation to deeply understand the microstructure of the remelted WC-Ni coatings. Fig. 2 shows the polished and the etched surfaces of the remelted WC-Ni coatings. The polished surface of the remelted WC-Ni coatings displayed a structure of Ni wrapped up in WC lamellae (Fig. 2a-c). After etching, the Ni was removed, clearly presenting the microstructure of the WC skeletons. The WC skeletons remained in their original shape, showing a 3D honeycomb skeleton structure (Fig. 2d-f). The magnified SEM images (Fig. 2g-i) indicate that the depth of the holes in these skeletons was followed by 500 W > 400 W > 300 W coatings. The difference between these coatings might affect the cavitation erosion resistance of the coatings.

Besides the differences in the microstructure for cold sprayed WC-Ni coatings and remelted WC-Ni coatings, the phase compositions and microhardness of the coatings before and after laser surface remelting were also investigated. The XRD patterns of the as-sprayed coating and the remelted coatings are shown in Fig. 3a. The peaks of the remelted WC-Ni coatings were similar to the WC-Ni coatings indicating the phase

structure of the WC-Ni coating after laser surface remelting did not change. However, the peaks slightly shifted to a lower angle after laser surface remelting, which could be attributed to the residual stresses in the remelted coatings. With the increase of laser power, the peak intensity of WC in the WC-Ni eutectic coatings became weaker, suggesting that the WC grain was refined [30]. The microhardness of the specimens was presented in Fig. 3b, showing slight changes in the specimens before and after remelting. The hardness of the 300 W and the 500 W coatings was slightly reduced compared with the 400 W coating. For the 300 W coating, the reduction in microhardness could be attributed to the less precipitated lamellar WC grains due to the incomplete melting of the WC particles by insufficient laser power (Fig. 1b). For the 500 W coating, even a dense distribution of the WC lamellae was observed, the increased porosity in the 500 W coating could be the possible reason for the decreased microhardness (Fig. 1d).

3.2. Cumulative volume loss

The cavitation erosion resistance of the cold sprayed WC-Ni coatings and remelted WC-Ni coatings was investigated according to the cumulative volume loss and the volume loss rate (Fig. 4). The cumulative

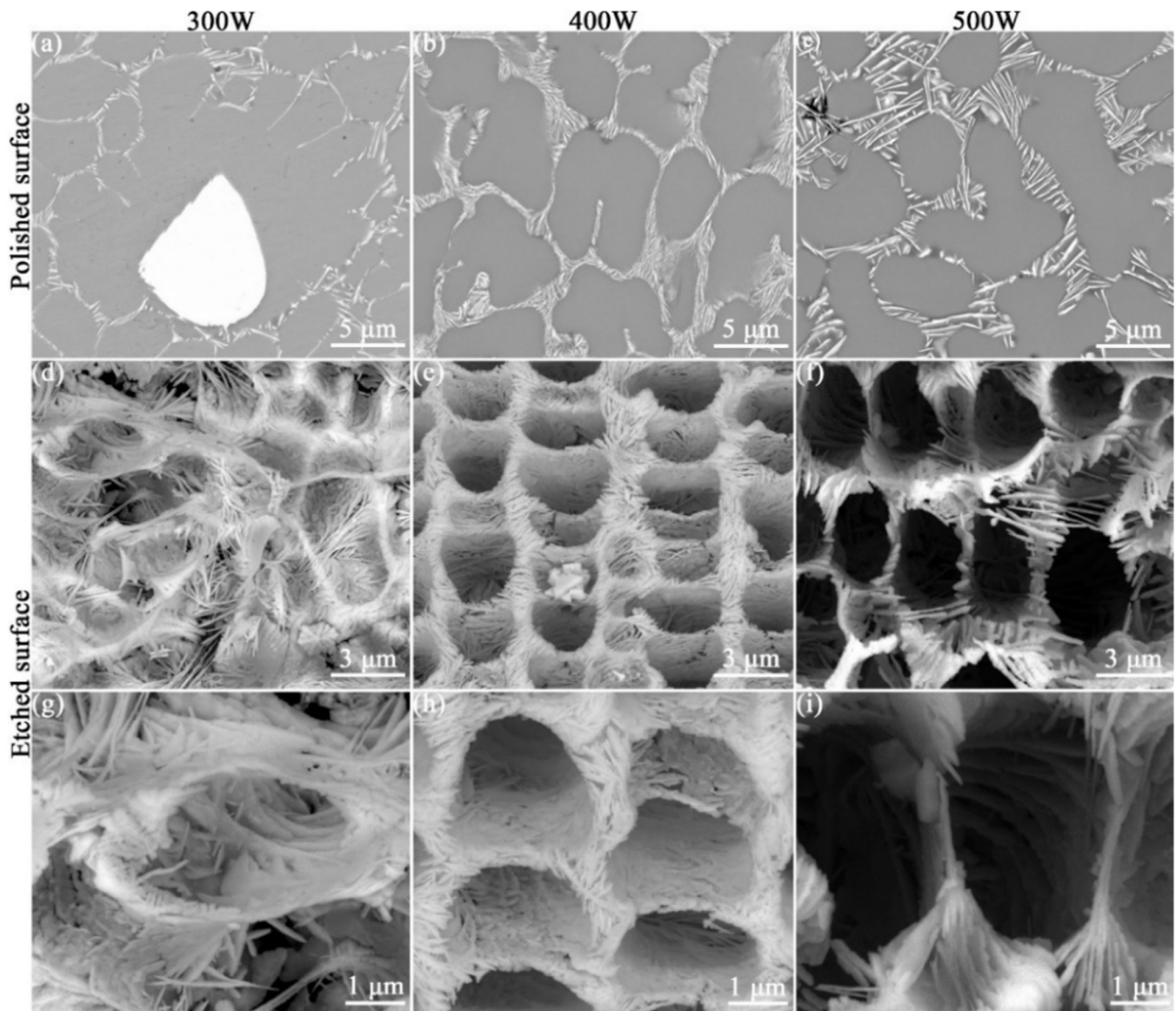


Fig. 2. SEM images of the polished surfaces (a-c) and the etched surfaces (d-i) of the remelted WC-Ni coatings.

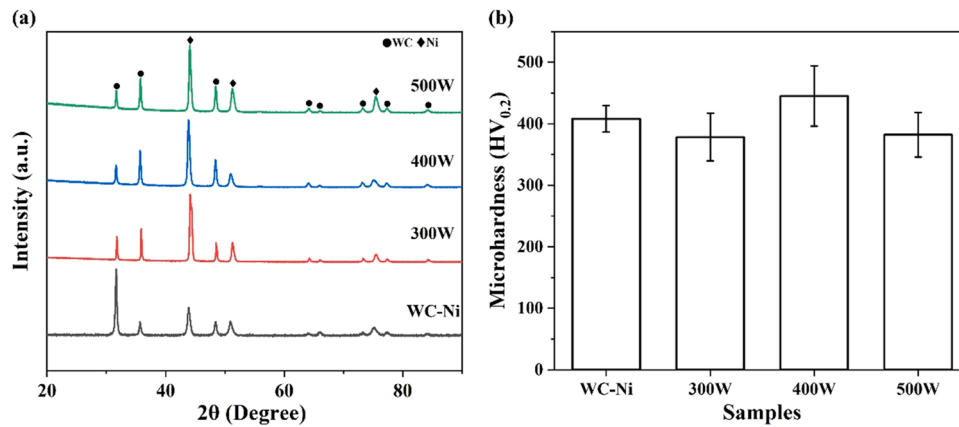


Fig. 3. (a) XRD patterns and (b) microhardness of cold sprayed WC-Ni coating, 300 W, 400 W, and 500 W coatings.

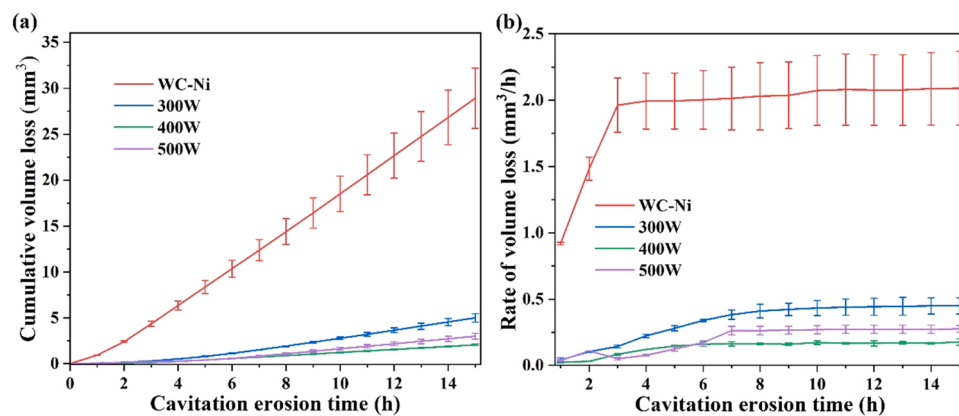


Fig. 4. (a) Cumulative volume loss and (b) the volume loss rates of the as-sprayed WC-Ni coating and the remelted WC-Ni coatings during cavitation erosion.

volume loss of the WC-Ni coating, the 300 W, 400 W, and 500 W coatings over 15 h of erosion was approximately 28.92, 5.01, 2.07, and 3.01 mm³, respectively (Fig. 4a). Fig. 4b shows the volume loss rates versus cavitation time. The WC-Ni coating presented the highest loss rate, and its cavitation erosion resistance was the worst among all these specimens. All the remelted coatings exhibited lower volume loss, which indicated that the cavitation erosion resistance of the WC-Ni coating was enhanced after the laser surface remelting. The best performance of the 400 W coatings in cavitation erosion resistance could be probably related to its higher hardness (Fig. 3b). However, considering all these remelted coatings significantly improved cavitation erosion resistance, the unique microstructure of the laser treated coatings (Fig. 2) might be the decisive reason for the cavitation erosion resistance improvement. Moreover, the cumulative volume loss and volume loss rate of the 300 W coating were higher than that of other remelted coatings. The 400 W coating had a better performance than the 500 W coating. The XRD results indicated that the composition in the remelted layer was not changed (Fig. 3a). Therefore, the cavitation erosion resistance difference among these coatings could be attributed to the structural differences.

The surface profiles of the specimens after cavitation erosion were investigated to better understand the cavitation erosion behaviour of the coatings. The surface roughness of the specimen from high to low was followed by the as-sprayed WC-Ni, 300 W, 400 W, and 500 W coatings, which could be explained by the difference in the shape of cavitation pits. For the WC-Ni coatings, large pits could be observed from the eroded surface after cavitation erosion (Fig. 5a-1). These pits were about 80 μm in depth (Fig. 5a-2) and much deeper than that of the remelted coatings. The cavitation pits were about 10 μm in depth for the 300 W and the 500 W coatings, while a few of deep pits could still be observed

in the 300 W coatings (Fig. 5b-2 and d-2). The cavitation pits in the 400 W coatings were much smaller than all other specimens (Fig. 5c-1), whose depth was less than 10 μm (Fig. 5c-2).

To further investigate the surface profile, Abbott-Firestone curves of the eroded surface after cavitation erosion were provided, and the corresponding Sv values were also calculated (Fig. 6). Through the statistics for the depth distribution of the eroded surfaces, it could be confirmed that the cavitation pits exhibited various dimensions. Moreover, the Sv values of the cold-sprayed WC-Ni, 300 W, 400 W and 500 W coatings were 80.2, 27.8, 10.6, and 13.8 μm, respectively, which is consistent with the cavitation erosion results indicated by the plots in Fig. 4. Severe cavitation damage occurred in the WC-Ni coatings during cavitation erosion, but the damage was limited in all these remelted coatings. The depth of the cavitation pits in the 400 W coating was smaller than that in the other coatings. This result indicates that the 400 W coating showed higher cavitation erosion resistance than other coatings, corresponding to the cumulative volume loss and the volume loss rate results (Fig. 4). Therefore, we proposed that the hindered formation of the cavitation pit could be the possible reason for the enhanced cavitation erosion resistance, but the specific mechanism was still unknown.

For a better understanding of the cavitation erosion resistance mechanism of the laser surface remelted coatings, the structure evolution of the coatings during cavitation erosion was investigated. Fig. 7 shows the cross-sectional morphology of the as-sprayed WC-Ni coating and the remelted WC-Ni coatings after cavitation erosion for 15 h, demonstrating the propagation process of cavitation erosion pits. For the as-sprayed WC-Ni coatings, a cavitation erosion pit formed in the Ni matrix (Fig. 7a). The propagation of the cavitation erosion pit in the Ni matrix was both parallel and vertical to the surface. After the cavitation

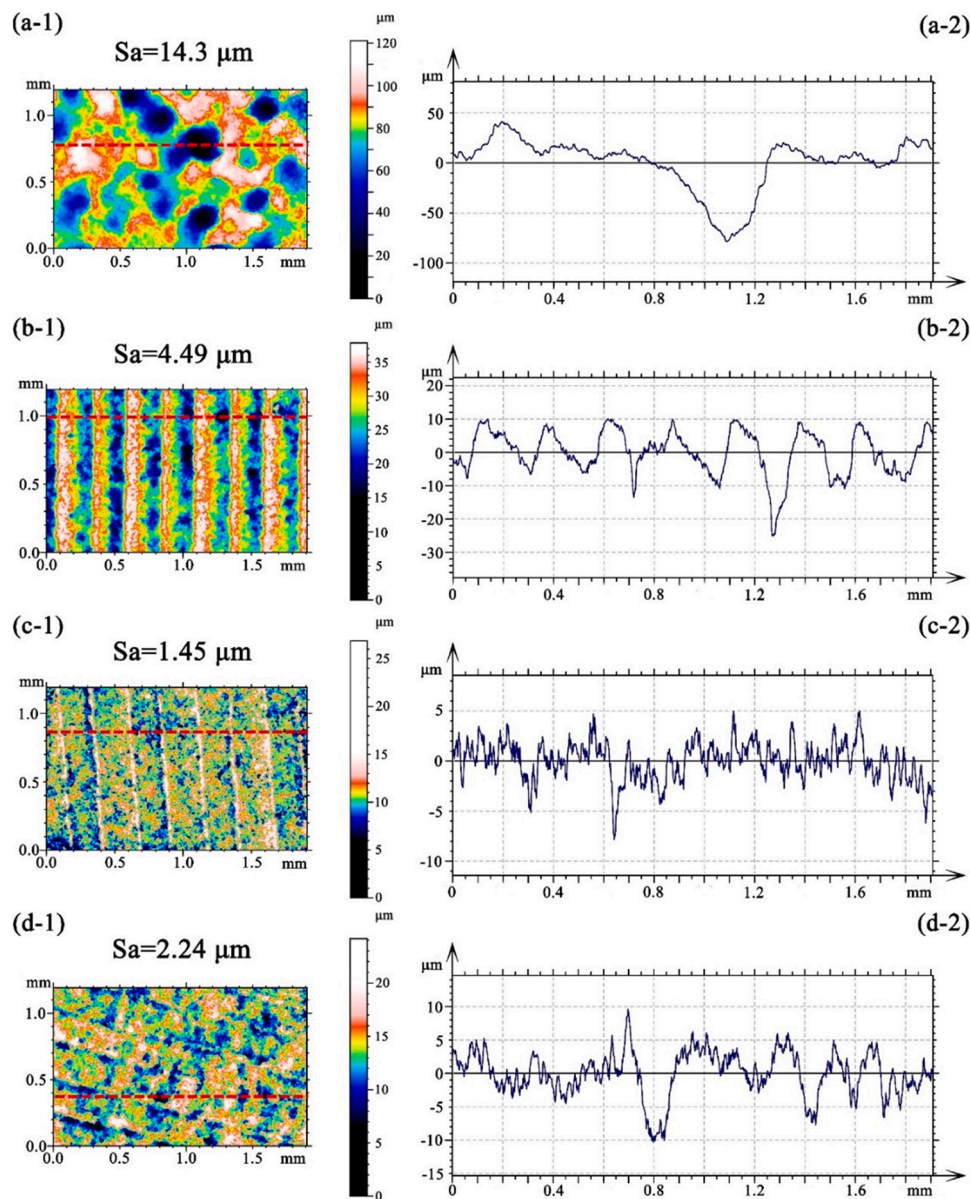


Fig. 5. Surface (–1) and linear (–2) profiles of the cold sprayed WC-Ni coating (a), 300 W (b), 400 W (c), and 500 W (d) coatings after cavitation erosion testing.

erosion for 15 h, the Ni was removed, but the WC remained. This result indicates that the binder phases of Ni might be more easily damaged, and the hard phases of WC could hinder the propagation of cracks. Fig. 7b-d shows that the cavitation erosion pits and crack propagation occurred in the Ni binder phase. This phenomenon suggested that the WC lamellae transformed from WC particles could also hinder the propagation of the cracks and cavitation erosion pits. However, the cavitation erosion pits in the remelted coatings were smaller than those in the as-sprayed coating. The distribution of the WC was more even in the remelted coatings, resulting in the propagation of the cracks and cavitation erosion pits became more difficult. Therefore, the remelted WC-Ni coatings were more resistant to cavitation erosion. For the 300 W coating, however, the unmelted WC particles remained, and the binder phase of Ni was incompletely surrounded by the WC lamella (Fig. 7b). The cracks were easy to grow through the weak area of the WC-Ni interfaces. Therefore, the 300 W coating was less resistant to cavitation erosion than the other remelted coatings. With the increase of laser power, the WC skeleton was more evenly distributed in the coating. Meanwhile, the high laser power of 400 W probably improved the bonding strength of WC and Ni. Cracks were difficult to propagate along

with the WC-Ni interfaces (Fig. 7c and d). Consequently, the 400 W coating showed better cavitation erosion resistance (Fig. 7c). For the 500 W coatings, the cracks propagated both in and along with the WC skeleton, while the crack propagation in the WC skeleton was hindered. However, the cavitation erosion resistance of the 500 W coating decreased. The SEM images of the 500 W coating showed that the WC skeletons were larger than that in the 400 W coatings, offering an easy propagation path for cracks. In addition, there were many pores in the 500 W coating, which could also adversely affect the cavitation erosion resistance [24–26].

The laser surface melted WC-Ni coatings with WC skeleton structure exhibited excellent cavitation erosion resistance (Fig. 7). Due to a uniform dispersion of WC lamellae which prevented the crack propagation, the cracks in the remelted coatings were much smaller than that in the as-sprayed coatings (Fig. 7), but the weak area of the WC skeleton could destroy the WC skeleton structure during the cavitation erosion (Fig. 7b and c). Fig. 8 presents the surfaces of the etched 400 W coating before and after cavitation erosion for 5 min, showing that the exposed WC skeleton was removed from the surface after only 5 min of cavitation erosion (Fig. 8b). It was indicated that the pure WC skeleton was easily

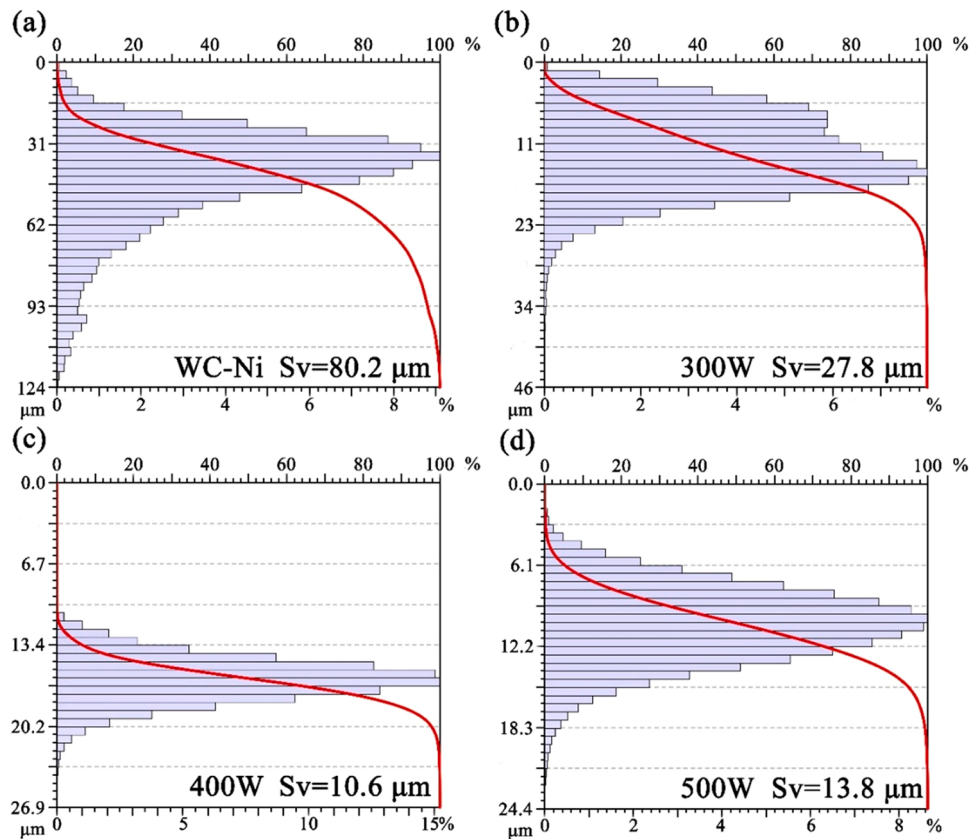


Fig. 6. Abbott-Firestone curves (the red curves) and depth distributions (the purple columns) of the cold sprayed WC-Ni coating (a), 300 W (b), 400 W (c), and 500 W (d) coatings after cavitation erosion testing.

damaged under the cavitation erosion impact.

The results of the cavitation erosion test and the SEM observation show that there was a significant improvement in the cavitation erosion resistance of the WC-Ni coating after laser surface remelting. Ni was preferentially damaged during the cavitation process, while the WC particle and the WC lamellae could restrict the cavitation erosion damage. However, pure WC skeletons could be removed after being exposed to cavitation erosion for several minutes (Fig. 8). These results illustrate that the WC skeleton could hinder the propagation of cavitation erosion, and the Ni could protect the WC skeleton from being removed. Therefore, the cavitation erosion resistance of the remelted WC-Ni coatings was thought to be primarily determined by the combined effects of the Ni binder phase and the WC skeleton.

3.3. Evolution of defects in WC-Ni eutectic coatings

Generally, defects (such as pores) in materials negatively affect the cavitation erosion resistance [27]. The evolution of pores was observed by SEM observation. For the 300 W coating (Fig. 9a), the pores were mainly distributed in the WC skeleton (Fig. 1b) and grew along with the WC skeleton during the first 15 h of cavitation erosion (Fig. 9a-3, a-4 and a-5). After 15 h of erosion, the pore not only grew along with the WC skeleton but also propagated to the Ni. The evolution of pores in the 400 W coating was different. The pore grew in the Ni matrix during the first 6 h (Fig. 9b-3). However, the propagation of the pore stopped when further exposed to cavitation erosion, and the pore shrunk after 20 h of cavitation erosion (Fig. 9b-4, b-5 and b-6).

For the 500 W coating, the pores were distributed in both the WC skeleton and the WC-Ni interfaces (Fig. 1d). The pores in the WC skeleton grew along with the WC skeleton in the first 6 h (Fig. 10a-2, a-3 and a-4). When the coating was exposed to cavitation erosion further, the propagation of the pores was hindered by the WC lamellae (Fig. 10a-5

and a-6). For the pores at the WC-Ni interfaces, they expanded in both Ni and WC skeleton in the first 10 h (Fig. 10b-2, b-3, b-4 and b-5) and shrunk (Fig. 10b-6) after the further exposure to cavitation erosion.

Based on the SEM observations, the pre-existing pores in the WC skeleton would grow along with the skeleton (Figs. 9a and 10a) during the cavitation erosion. With the increase of cavitation erosion time, these pores could grow in the Ni (Fig. 10a-5 and a-6). Considering the cracks could grow through the weakness of the WC skeleton under the cavitation exposure (Fig. 7 b-d), we propose that these pores would accelerate the material failure after further erosion. Although these pores expanded initially, they would shrink when exposed to cavitation erosion further (Figs. 9b and 10b). The shrinkage of these pores could be possibly attributed to the deformation of Ni. After hours of cavitation erosion test, the Ni around the pores might deform due to the bubble collapse impact, resulting in the shrinkage of pores. A similar phenomenon in stainless steel was observed in our previous study [31]. Furthermore, the pores in the WC lamella could not shrink during the cavitation erosion process possibly due to the deformation being blocked by the WC lamella, and the 300 W coating with more pores in the WC lamellae showed relatively lower cavitation erosion resistance than the other remelted coatings.

4. Conclusions

The cavitation erosion behaviour of the cold sprayed WC-Ni coating and the laser surface melted WC-Ni coatings were studied by the SEM observation. The cavitation erosion mechanism of the laser surface melted WC-Ni coatings was discussed. In addition, the evolution of the pores in the laser surface melted WC-Ni coatings was observed by SEM at the same locations. The main conclusions were summarized below:

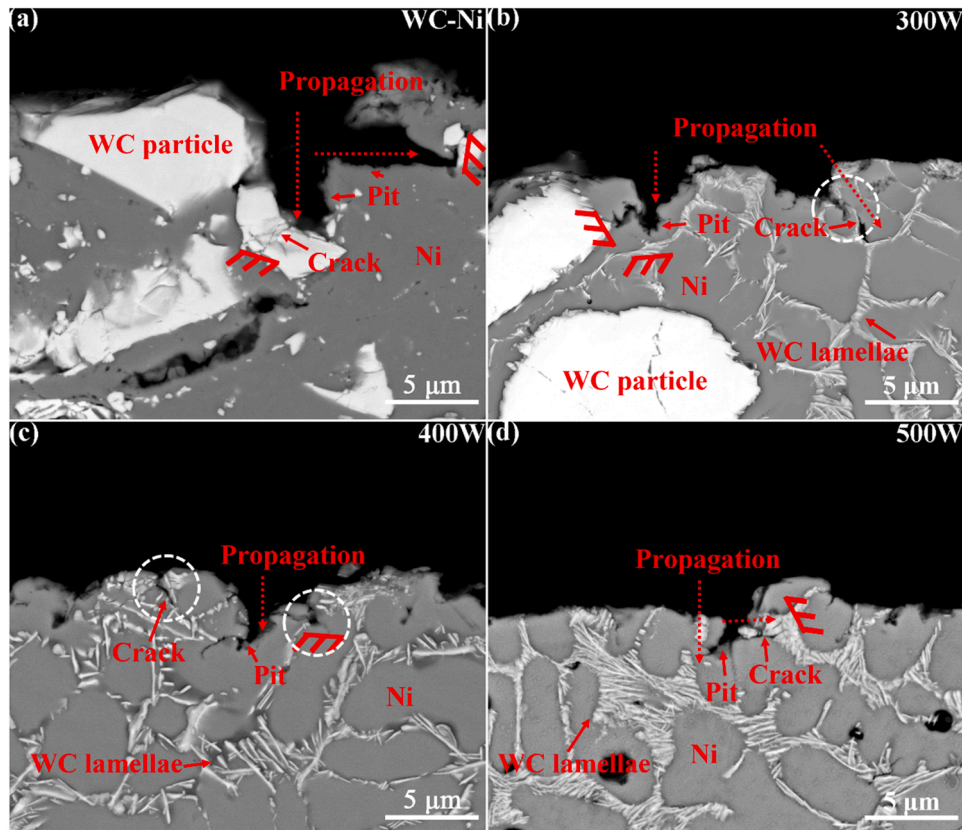


Fig. 7. The cross-sectional morphology of the as-sprayed WC-Ni coating (a), 300 W (b), 400 W (c), and 500 W (d) coatings after 15 h of cavitation erosion testing. The cavitation erosion pits and the cracks were highlighted by red arrows; the propagation of cavitation erosion pit was highlighted by red dot arrows; the weakness of the WC skeleton was highlighted by white dot circles; the fence represented the propagation of the cavitation erosion pit hindered in this direction.

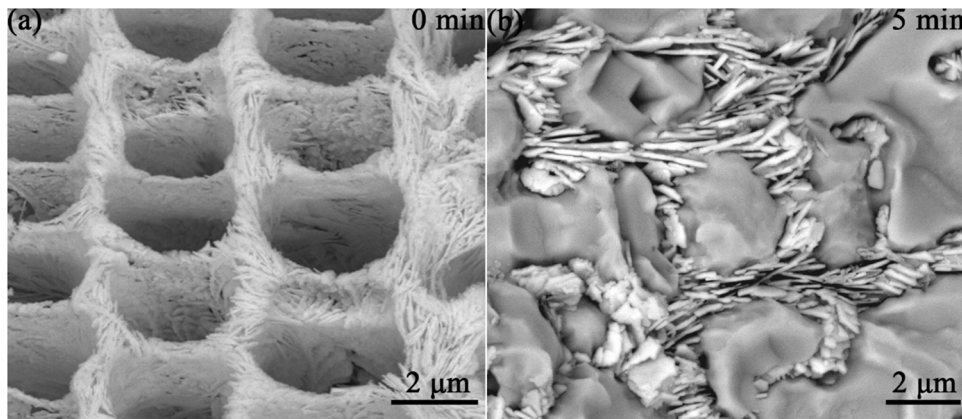


Fig. 8. SEM images of the etched surfaces of the 400 W coating before (a) and after (b) cavitation erosion. The specimens were exposed to cavitation erosion for 5 min.

- (1) It was found that the cold sprayed WC-Ni coating had a better cavitation erosion resistance than pure the Ni due to the WC particles could hinder the propagation of cracks and pits.
- (2) The cavitation erosion resistance of the as-sprayed WC-Ni coating was further improved after laser surface melting at different laser power. The 400 W coating with evenly distributed WC skeleton exhibited better cavitation erosion resistance than the 300 W and 500 W coatings.
- (3) The pure WC skeleton was destroyed rapidly under the cavitation erosion, indicating that the great performance of the remelted WC-Ni coatings was attributed to the synergistic effect of the hard phase and binder phase.

Statement of originality

The authors assure that the contents of this contribution are original, and this paper has not been submitted to any other journal for publication, or not published before elsewhere, and this article contains no libelous or unlawful statements, and does not infringe on the rights of others.

Declaration of Competing Interest

The authors declare that they have no known competing financial interests or personal relationships that could have appeared to influence

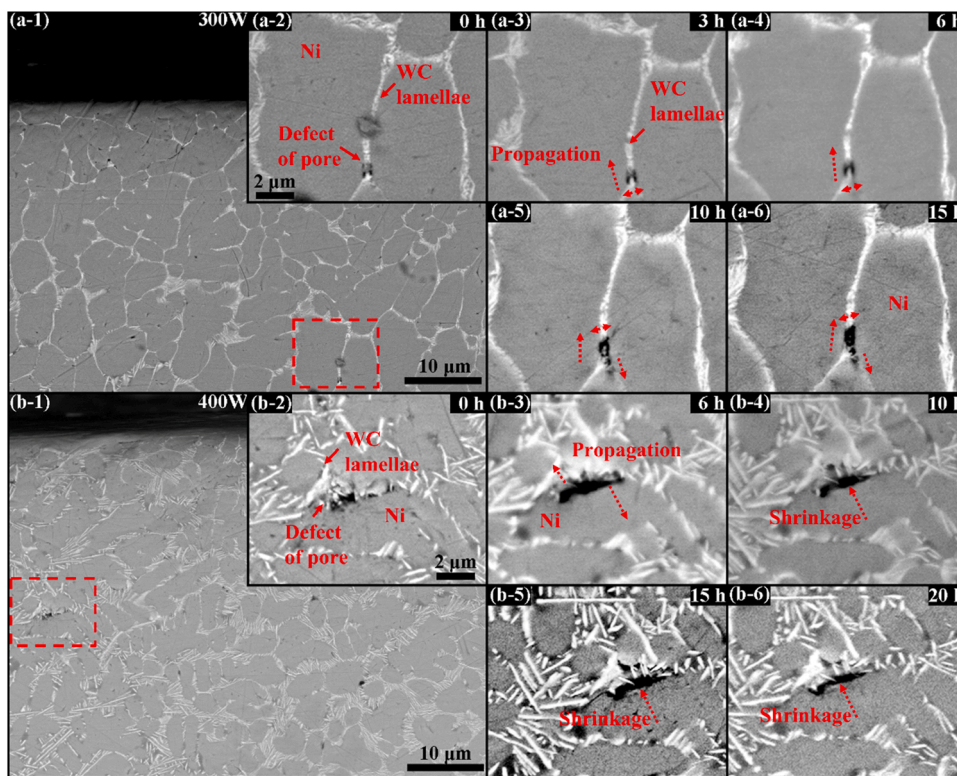


Fig. 9. Typical SEM cross-sectional morphologies of the 300 W (a) and the 400 W (b) coatings after different cavitation erosion times at the same observation point. The evolution of pores was highlighted by red dot arrows.

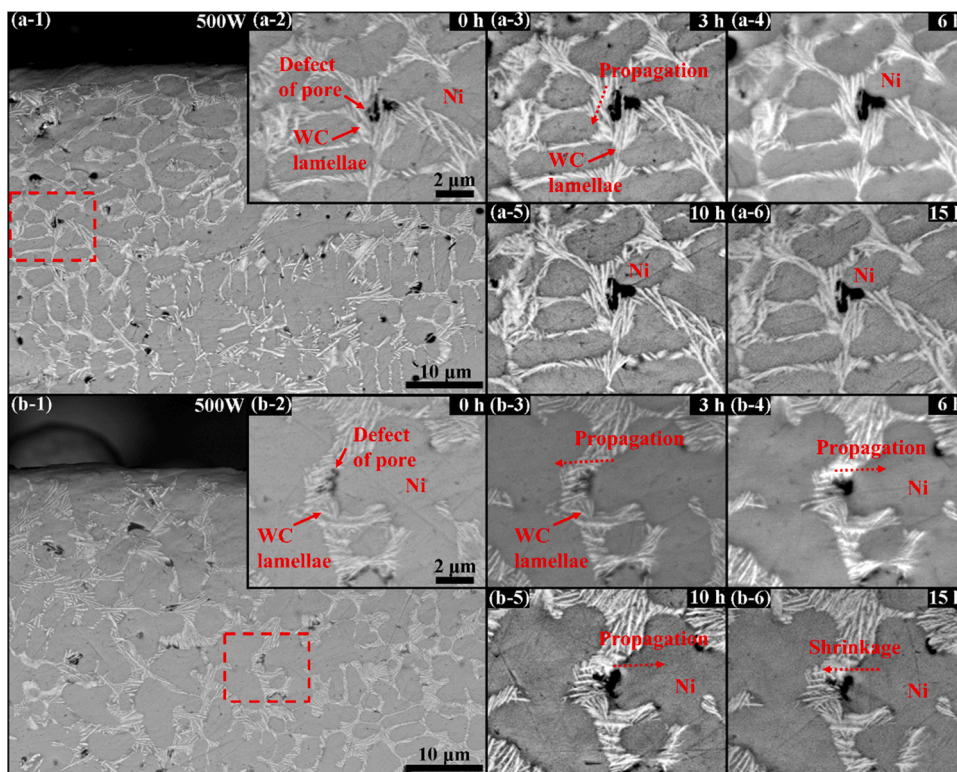


Fig. 10. Typical SEM cross-sectional morphologies of the 500 W coating after different erosion times at the same observation point, showing the evolution process of the pores in the WC skeleton (a) and at the WC-Ni interfaces (b).

the work reported in this paper.

Acknowledgements

This work was supported by the Zhejiang Provincial Natural Science Foundation of China (grant #LZ22E090001), Ningbo 3315 Talents Program (grant #2020A-29-G), Ningbo Science and Technology Innovation 2025 Major Program (grant #2020Z086), and Special Foundation for Postgraduate Innovation in Jiangxi Province (YC2020-S458).

References

- [1] Alfonso S, Gesto M, Sadoul B. Temperature increase and its effects on fish stress physiology in the context of global warming. *J Fish Biol* 2021;98:1496–508. <https://doi.org/10.1111/jfb.14599>.
- [2] Gutiérrez-Gamboa G, Zheng W, de Toda FM. Current viticultural techniques to mitigate the effects of global warming on grape and wine quality: a comprehensive review. *Food Res Int* 2021;139:109946. <https://doi.org/10.1016/j.foodres.2020.109946>.
- [3] Yamaguchi M, Chan JC, Moon I-J, Yoshida K, Mizuta R. Global warming changes tropical cyclone translation speed. *Nat Commun* 2020;11:1–7. <https://doi.org/10.1038/s41467-019-13902-y>.
- [4] Elavarasan RM, Shafiullah G, Padmanaban S, Kumar NM, Annam A, Vetrichelvan AM, et al. A comprehensive review on renewable energy development, challenges, and policies of leading Indian states with an international perspective. *IEEE Access* 2020;8:74432–57. <https://doi.org/10.1109/ACCESS.2020.2988011>.
- [5] Pehl M, Arvesen A, Humpenöder F, Popp A, Hertwich EG, Luderer G. Understanding future emissions from low-carbon power systems by integration of life-cycle assessment and integrated energy modelling. *Nat Energy* 2017;2:939–45. <https://doi.org/10.1038/s41560-017-0032-9>.
- [6] Llamas C, Sovacool BK. The future of hydropower? A systematic review of the drivers, benefits and governance dynamics of transboundary dams. *Renew Sust Energy Rev* 2021;137:110495. <https://doi.org/10.1016/j.rser.2020.110495>.
- [7] Nautiyal H, Goel V. Sustainability assessment of hydropower projects. *J Clean Prod* 2020;265:121661. <https://doi.org/10.1016/j.jclepro.2020.121661>.
- [8] Kahraman G, Taşgin Y. Application of local hard fillet weld to repair damage caused by cavitation in hydroelectric power plant. *J Fail Anal Prev* 2020;20:912–9. <https://doi.org/10.1007/s11668-020-00892-z>.
- [9] Babu A, Perumal G, Arora H, Grewal H. Enhanced slurry and cavitation erosion resistance of deep cryogenically treated thermal spray coatings for hydroturbine applications. *Renew Energy* 2021;180:1044–55. <https://doi.org/10.1016/j.renene.2021.09.006>.
- [10] Jiang X, Overman N, Smith C, Ross K. Microstructure, hardness and cavitation erosion resistance of different cold spray coatings on stainless steel 316 for hydropower applications. *Mater Today Commun* 2020;25:101305. <https://doi.org/10.1016/j.mtcomm.2020.101305>.
- [11] Kumar H, Chittosiya C, Shukla V. HVOF Sprayed WC based cermet coating for mitigation of cavitation, erosion & abrasion in hydro turbine blade. *Mater Today Proc* 2018;5:6413–20. <https://doi.org/10.1016/j.matpr.2017.12.253>.
- [12] Kumar R, Kamaraj M, Seetharamu S, Pramod T, Sampathkumaran P. Effect of spray particle velocity on cavitation erosion resistance characteristics of HVOF and HVOF processed 86WC-10Co4Cr hydro turbine coatings. *J Therm Spray Technol* 2016;25:1217–30. <https://doi.org/10.1007/s11666-016-0427-3>.
- [13] Lamana MS, Pukaszewicz AG, Sampath S. Influence of cobalt content and HVOF deposition process on the cavitation erosion resistance of WC-Co coatings. *Wear* 2018;398:209–19. <https://doi.org/10.1016/j.wear.2017.12.009>.
- [14] Lima M, Godoy C, Modenesi P, Avelar-Batista J, Davison A, Matthews A. Coating fracture toughness determined by Vickers indentation: an important parameter in cavitation erosion resistance of WC-Co thermally sprayed coatings. *Surf Coat Technol* 2004;177:489–96. [https://doi.org/10.1016/S0257-8972\(03\)00917-4](https://doi.org/10.1016/S0257-8972(03)00917-4).
- [15] Wu Y, Hong S, Zhang J, He Z, Guo W, Wang Q, et al. Microstructure and cavitation erosion behavior of WC-Co-Cr coating on 1Cr18Ni9Ti stainless steel by HVOF thermal spraying. *Int J Refract Metals Hard Mater* 2012;32:21–6. <https://doi.org/10.1016/j.ijrmhm.2012.01.002>.
- [16] Du J, Zhang J, Zhang C. Effect of heat treatment on the cavitation erosion performance of WC-12Co coatings. *Coatings* 2019;9:690. <https://doi.org/10.3390/coatings9100690>.
- [17] Hong S, Wu Y, Zhang J, Zheng Y, Qin Y, Gao W, et al. Cavitation erosion behavior and mechanism of HVOF sprayed WC-10Co-4Cr coating in 3.5 wt% NaCl solution. *Trans Indian Inst Met* 2015;68:151–9. <https://doi.org/10.1007/s12666-014-0440-5>.
- [18] Mateos J, Cuetos J, Fernandez E, Vijande R. Tribological behaviour of plasma-sprayed WC coatings with and without laser remelting. *Wear* 2000;239:274–81. [https://doi.org/10.1016/S0043-1648\(00\)00325-2](https://doi.org/10.1016/S0043-1648(00)00325-2).
- [19] Zhou S, Xu Y, Liao B, Sun Y, Dai X, Yang J, et al. Effect of laser remelting on microstructure and properties of WC reinforced Fe-based amorphous composite coatings by laser cladding. *Opt Laser Technol* 2018;103:8–16. <https://doi.org/10.1016/j.optlastec.2018.01.024>.
- [20] Song Q, Tong Y, Li H, Zhang H, Xu N, Zhang G, et al. Corrosion and cavitation erosion resistance enhancement of cast Ni-Al bronze by laser surface melting. *J Iron Steel Res Int* 2021:1–11. <https://doi.org/10.1007/s42243-021-00674-3>.
- [21] Suresh G, Dasgupta A, Kishor P, Upadhyay B, Saravanan T, Mallika C, et al. Effect of laser surface melting on the microstructure and pitting corrosion resistance of 304L SS weldment. *Metall Mater Trans B* 2017;48:2516–25. <https://doi.org/10.1007/s11663-017-1049-y>.
- [22] Tang C, Cheng F, Man HC. Improvement in cavitation erosion resistance of a copper-based propeller alloy by laser surface melting. *Surf Coat Technol* 2004;182:300–7. <https://doi.org/10.1016/j.surfcoat.2003.08.048>.
- [23] da Silva MR, Gargarella P, Gustmann T, Botta Filho WJ, Kiminami CS, Eckert J, et al. Laser surface remelting of a Cu-Al-Ni-Mn shape memory alloy. *Mater Sci Eng A* 2016;661:61–7. <https://doi.org/10.1016/j.msea.2016.03.021>.
- [24] Ghadami F, Sohi MH, Ghadami S. Effect of TIG surface melting on structure and wear properties of air plasma-sprayed WC-Co coatings. *Surf. Coat Technol* 2015; 261:108–13. <https://doi.org/10.1016/j.surfcoat.2014.11.050>.
- [25] Chikarakara E, Aqida S, Brabazon D, Naher S, Picas J, Punset M, et al. Surface modification of HVOF thermal sprayed WC-CoCr coatings by laser treatment. *Int J Mater Form* 2010;3:801–4. <https://doi.org/10.1007/s12289-010-0891-0>.
- [26] Yang R, Tian Y, Huang N, Lu P, Chen H, Li H, et al. Effects of CeO₂ addition on microstructure and cavitation erosion resistance of laser-processed Ni-WC composites. *Mater Lett* 2021;311:131583. <https://doi.org/10.1016/j.matlet.2021.131583>.
- [27] Zhang H, Chen X, Gong Y, Tian Y, McDonald A, Li H. In-situ SEM observations of ultrasonic cavitation erosion behavior of HVOF-sprayed coatings. *Ultrason Sonochem* 2020;60:104760. <https://doi.org/10.1016/j.ultsonch.2019.104760>.
- [28] Zhou S, Dai X, Zheng H. Microstructure and wear resistance of Fe-based WC coating by multi-track overlapping laser induction hybrid rapid cladding. *Opt Laser Technol* 2012;44:190–7. <https://doi.org/10.1016/j.optlastec.2011.06.017>.
- [29] Qiu C, Adkins NJ, Attallah MM. Selective laser melting of Invar 36: microstructure and properties. *Acta Mater* 2016;103:382–95. <https://doi.org/10.1016/j.actamat.2015.10.020>.
- [30] Lima MJS, Souto M, Souza A, Karimi M, Silva F, Gomes UU, et al. Synthesis of nanostructured tungsten carbide (WC) from ammonia paratungstate-APT and its characterization by XRD and rietveld refinement. *Mater Sci Forum* 2017;899:31–5. <https://doi.org/10.4028/www.scientific.net/MSF.899.31>.
- [31] Tian Y, Zhao H, Yang R, Liu X, Chen X, Qin J, et al. In-situ SEM investigation on stress-induced microstructure evolution of austenitic stainless steels subjected to cavitation erosion and cavitation erosion-corrosion. *Mater Des* 2022;213:110314. <https://doi.org/10.1016/j.matdes.2021.110314>.